JCTC Journal of Chemical Theory and Computation

Article

pubs.acs.org/JCTC

Free Energy Reconstruction from Metadynamics or Adiabatic Free Energy Dynamics Simulations

Michel A. Cuendet[†,‡] and Mark E. Tuckerman*[,†]

[†]Department of Chemistry, New York University, New York, New York 10003, United States

[‡]Swiss Institute of Bioinformatics, UNIL Sorge, 1015 Lausanne, Switzerland

Supporting Information

ABSTRACT: In molecular dynamics simulations, most enhanced sampling methods are traditionally associated with one particular estimator to calculate the free energy surface (FES), such as the histogram, the mean force, or the bias potential. Here, we start from the realization that four enhanced sampling methods, metadynamics and well-tempered metadynamics (in their extended Lagrangian form), as well as driven adiabatic free energy dynamics (dAFED) and unified free energy dynamics (UFED), can be used in combination with any of the three above-mentioned FES estimators. We compare the convergence properties of these estimators on the alanine dipeptide and a sodium ion solvation shell. We find that the mean force estimator is superior in all cases. We also show that it can be marginally beneficial to combine information from the histogram and the force, provided that both are of comparable accuracy.

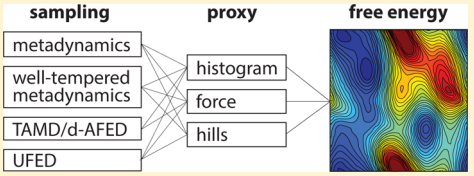

1. INTRODUCTION

One of the most challenging goals of molecular dynamics (MD) simulation is the calculation of free energy differences between slowly interconverting conformational states of systems such as polymers, biomolecules, or crystal polymorphs. To achieve this within a limited simulation time, enhanced sampling methods are required. These methods can either enhance sampling globally, for example, using replica exchange schemes, or instead, focus on a few collective variables (CVs) that are adequate to describe the reaction of interest.

Numerous algorithms[1,2] have been introduced to efficiently sample the space of one or a few CVs using MD. In general, a particular free energy method has two distinct components. The first is enhanced sampling, that is, a scheme to modify the system's dynamics to generate a sample of conformations that is not limited by free energy barriers. The second component is the subsequent procedure for reconstructing the FES based on the samples generated by the modified dynamics. In statistics, an *estimator* is a rule for calculating an estimate of a given quantity based on observed data. Therefore, we will call the second component of free energy methods the FES *estimator*.

Traditionally, enhanced sampling algorithms have been associated with one particular FES estimator that relates directly to the type of data the sampling algorithms most naturally generate (state density, thermodynamic force, work, etc.). We will call this primary sampled data the *proxy*, reserving the term *estimator* for the mathematical relation yielding the FES from the proxy, as there often exists more than one estimator based on a given proxy. To illustrate this point, we give a few examples of representative sampling methods and estimators most commonly associated with them.

Umbrella sampling[3] introduces a series of restraint potentials and uses the (unbiased) state density as the FES proxy and the weighted histogram method (WHAM)[4,5] as the FES estimator. The Blue Moon method[6,7] imposes constraints at fixed CV positions and uses the mean constraint force as a proxy to estimate the FES based on the old idea of thermodynamic integration.[8] The more recent adaptive biasing force method also uses the mean force[9,10] as a proxy. The reference potential spatial warping algorithm (REPSWA)[11,12] can use either the state density or mean force as the proxy. Another popular method, metadynamics,[13,14] is based on an adaptive biasing potential and traditionally uses the inverted final bias potential as the FES estimator. In nonequilibrium methods such as steered MD, the mechanical work applied on the system is the proxy to to construct a FES using, for example, the Jarzynski identity[15] as the estimator. Finally, we mention the tesselation milestoning method,[16] which uses a more unusual proxy, namely, counts of transitions across cell boundaries in the CV space.

Based on this classification, it would be possible to write a full review of known free energy methods, but this is not our aim here. Nevertheless, it is important to note that many combinations of sampling methods and proxies are possible across the categories mentioned above. For example, the umbrella integration method,[17] as well as the later gradient-augmented Fourier beads method[18] or the single sweep method,[19] involve restraint potentials characteristic of umbrella sampling but use the mean force as a proxy, together with a thermodynamic intergation-based estimator. As another example, several estimators have been recently proposed[20−23] to reweight adaptively the state density obtained from metadynamics simulations, which show improved performance

Received: January 7, 2014
Published: June 30, 2014

   dx.doi.org/10.1021/ct500012b | J. Chem. Theory Comput. 2014, 10, 2975−2986

compared to the traditional bias potential-based estimator and can provide ensemble averages of observables other than the CVs.

Here, we focus on four related enhanced sampling methods. The first is the well-established and widely used metadynamics[13,14] method, in which a bias potential is adaptively constructed during the simulation by depositing small gaussians (hills) in visited regions of the CV space. The second method is an improved version of the first, called well-tempered metadynamics,[24] in which the hill size is allowed to decrease as the simulation progresses to obtain better convergence properties. The third method is the temperature accelerated MD (TAMD) method,[25] also known as driven adiabatic free energy dynamics[26] (d-AFED) that originated from the earlier adiabatic free energy dynamics (AFED)[27,28] and canonical adiabatic free energy sampling (CAFES) methods.[29] The principle of the TAMD/d-AFED method is to couple the CVs to extended variables adiabatically decoupled from the physical system and maintained at high temperature, which drives the system over free energy barriers while allowing the FES to be constructed straightforwardly from the temperature-scaled state density. Note that ensemble averages of any observable can also be calculated from a TAMD/d-AFED simulation using a recently proposed reweighting scheme.[30] The fourth method is the recent unified free energy dynamics[31] (UFED), which combines the adaptive bias potential of metadynamics and the high-temperature, adiabatically separated extended variable scheme of TAMD/d-AFED. The argument behind UFED is that if the adiabatic separation is effective, the mean force in the CV space is independent of the state density. This means that the FES can be accurately estimated from the force, despite the alterations of the state density due to the high temperature and the hills.

In this work, we establish that each of metadynamics, well-tempered metadynamics, TAMD/d-AFED, and UFED can operate with the histogram, the mean force, or the hills (if applicable) as proxies. First we show, for the first time to our knowledge, that force-based FES estimators can be used with metadynamics or well-tempered metadynamics, provided that the extended-Lagrangian version of the methods[32] (including an extended dynamical variable) is used. Indeed, in this form, these schemes can be seen as special cases of UFED, and so can TAMD/d-AFED as well. In fact, we believe this is the first time an extended-Lagrangian version of the well-tempered metadynamics approach has been introduced. We then show that the histogram can be used as a proxy for UFED by deriving a high-temperature generalization of the histogram-reweighting method proposed in ref 23. for metadynamics. In addition, we show that the FES can be estimated from the hills in UFED, just as it is in metadynamics. After establishing that any proxy can be combined with any sampling method, we ask the question: for a given enhanced sampling scheme, which FES estimator is the most efficient? In other words, once a metadynamics, well-tempered metadynamics, TAMD/d-AFED, or UFED simulation has been run, which proxy should employed to get the most of our data: the histogram, the force, or the hills?

We go one step further and explore if combining information from the histogram and the force could lead to an improved FES estimator. For this, we resort to the regularized gradiant-enhanced kriging (GEK) regression method,[33−35] although one could also imagine using a Bayesian approach as an alternative. The advantage of regularized GEK over other existing regression methods is that it automatically assigns the relative importance of the gradient versus the data points in a parameter-free fashion.

We report the performance of the combined free energy methods on two systems. The first is the "hydrogen atom of enhanced sampling", the alanine dipeptide in vacuo. This simple system with high free energy barriers allows us to test extensively the effect of various simulation parameters. Second, we study the FES of one water molecule as a function of its distance to a sodium ion in solution, as an example of a system with sharp free energy features and many degrees of freedom orthogonal to the CV.

The paper is organized as follows. We begin by briefly reviewing the various FES estimators and how they are applied within each free energy method. In sections 2 and 3, we present FES convergence results for the alanine dipeptide and the sodium ion in water, respectively, and we discuss our observations in the Conclusions section. The generalized UFED reweighting scheme is given in Appendix A, and the generalized GEK regression algorithm is outlined in Appendix B.

Potential of Mean Force. Consider a system of N particles evolving at constant temperature T in a fixed volume of $\mathbb{R}^3$. Let $\mathbf{r} \in \mathbb{R}^{3N}$ be the positions of the N particles in a Cartesian reference frame. The physics of the system is encoded in the potential energy function $U(\mathbf{r})$. In order to describe a configurational transformation of interest, we define a set of n collective variables (CVs), that is, functions $\mathbf{q}$: $\mathbf{r} \rightarrow \mathbf{q}(\mathbf{r})$ mapping the coordinate space to the CV space of dimension $n \ll 3N$. The probability $\rho(\mathbf{s})$ of observing the system at a given value of the CVs, $\mathbf{q}(\mathbf{r}) = \mathbf{s}$ and the associated potential of mean force (PMF) $\phi(\mathbf{s})$ are defined by

$$\rho(\mathbf{s}) = \mathrm{e}^{-\beta\phi(\mathbf{s})} = \frac{1}{Z}\int d^N\mathbf{r}\, \mathrm{e}^{-\beta U(\mathbf{r})}\delta^{(n)}(\mathbf{q}(\mathbf{r}) - \mathbf{s}) \tag{1}$$

where we use a short-hand notation for the multidimensional Dirac δ-function, $\delta(\mathbf{q}(\mathbf{r}) - \mathbf{s}) = \prod_{i=1}^{n}\delta(q_i(\mathbf{r}) - s_i)$. Z is the configurational partition function of the physical system and $\beta = 1/k_\mathrm{B}T$.

In the TAMD/d-AFED scheme,[25,26] the multidimensional δ-function in eq 1 is replaced with a multidimensional Gaussian whose width tends to zero, which essentially amounts to substituting the constraint $\mathbf{q}(\mathbf{r}) = \mathbf{s}$ with a tight harmonic restraint with a diagonal force constant matrix $\mathbf{K}_s$. In addition, the Gaussian centers $\mathbf{s}$ are propagated, either by viewing them as extended phase-space variables and introducing conjugate momenta for them to be used within a thermostated MD scheme[26] or by sampling them via overdamped Langevin dynamics.[25] Introducing the integration over $\mathbf{s}$, the right-hand side of eq 1 becomes the configurational partition function

$$\tilde{Z} = \int d^n\mathbf{s}\int d^N\mathbf{r}\,\exp\left\{-\beta\left[U(\mathbf{r}) + \frac{1}{2}(\mathbf{q}(\mathbf{r}) - \mathbf{s})^T\mathbf{K}_s(\mathbf{q}(\mathbf{r}) - \mathbf{s})\right]\right\} \tag{2}$$

of an extended system with $\mathbf{s}$ adding n additional degrees of freedom to the configuration space. If we assign to $\mathbf{s}$ a diagonal mass matrix $\mathbf{M}_s$ whose elements are much larger than the effective masses of the CVs, the evolution of $\mathbf{s}$ becomes adiabatically decoupled from $\mathbf{r}$ and can be subjected to a heat bath at temperature $T_s > T$. The standard free energy estimator

in TAMD/d-AFED is based on the state density $\rho_{\mathrm{adb}}(\mathbf{s})$ in the adiabatic ensemble and takes the form

$$\phi^{\mathrm{adb}}(\mathbf{s}) = -k_{\mathrm{B}}T_s \ln[\rho_{\mathrm{adb}}(\mathbf{s})] \tag{3}$$

Note that for a one-dimensional CV, the effective mass is given[2] by

$$m_{\mathrm{eff}} = \left[\sum_{j=1}^{N} \frac{1}{m_j}\left(\frac{\mathrm{d}q}{\mathrm{d}\mathbf{r}_j}\right)^2\right]^{-1} \tag{4}$$

Note also that the mass that dictates the time scale of the coupling term appearing in eq 2 is the reduced mass $\mu = [1/m_{\mathrm{eff}} + 1/m_s]^{-1}$, which is approximately equal to m_{eff} when m_s is large. In the simple case where $q(\mathbf{r}) = x_1$, the x-coordinate of the first particle, we have $m_{\mathrm{eff}} = m_1$ and $\mu \approx m_1$, which means that the relevant time scale for thermostatting the extended system is dictated by the physical system mass, not by the large extended variable mass m_s.

In the recent UFED method,[31] the adiabatic approach is combined with an adaptive biasing potential $u^{\mathrm{bias}}(\mathbf{s},t)$ composed of small multidimensional Gaussian functions of height h and width σ gradually added along the extended variable trajectory $\mathbf{s}(t)$ at times t_i

$$u^{\mathrm{bias}}(\mathbf{s}, t) = \sum_{t_i<t} h\, \mathrm{e}^{-(\mathbf{s}-\mathbf{s}(t_i))^2/2\sigma^2} \tag{5}$$

This drastically modifies the state density, but it was shown[31] that, under adiabatic conditions, the force $\mathbf{f}(\mathbf{r},\mathbf{s})$ exerted by the physical system on $\mathbf{s}$ is not affected on average. It follows that the mean force can be used as a proxy for a free energy estimator, $\phi^{\mathrm{force}}(\mathbf{s})$, that satisfies

$$\nabla\phi^{\mathrm{force}}(\mathbf{s}) = -\langle \mathbf{f}(\mathbf{r}, \mathbf{s})\rangle_{\mathbf{s}}^{\mathrm{adb}} \tag{6}$$

where $\langle\cdot\rangle_{\mathbf{s}}^{\mathrm{adb}}$ represents an average in the adiabatic ensemble at (or in the vicinity of) a fixed value of $\mathbf{s}$. In order to reconstruct $\phi^{\mathrm{force}}(\mathbf{s})$, the mean force $\langle \mathbf{f}(\mathbf{r},\mathbf{s})\rangle_{\mathbf{s}}^{\mathrm{adb}}$ computed from the trajectory can either be integrated numerically on a grid or fitted to the coefficients of $\phi^{\mathrm{force}}(\mathbf{s})$ in a basis set expansion.

The equations of motion for UFED sampling are

$$\begin{aligned} m_i\ddot{\mathbf{r}}_i &= -\frac{\partial U}{\partial \mathbf{r}_i} + \sum_{\alpha=1}^{n} \kappa_\alpha(s_\alpha - q_\alpha(\mathbf{r}))\frac{\partial q_\alpha}{\partial \mathbf{r}_i} + \mathrm{Bath}(T) \\ \mu_\alpha\ddot{s}_\alpha &= -\kappa_\alpha(s_\alpha - q_\alpha(\mathbf{r})) - \frac{\partial u^{\mathrm{bias}}(\mathbf{s}, t)}{\partial s_\alpha} + \mathrm{Bath}(T_s) \end{aligned} \tag{7}$$

Here, μ_α, $\alpha = 1,\ldots,n$, are the diagonal elements of the mass matrix $\mathbf{M}_s$, and κ_α are the diagonal elements of the matrix $\mathbf{K}_s$. The physical particles are coupled to a thermal bath at temperature T while the extended system is coupled to a bath at temperature T_s. The bath can be of any type, for example, Langevin, Nosé–Hoover chains,[36] generalized Gaussian moment thermostatting (GGMT),[37] etc. The use of the high temperature T_s ensures that barriers on the FES can be easily crossed, and this process is further accelerated by the application of the bias potential in eq 5. Note that when $u^{\mathrm{bias}} = 0$, the UFED equations reduce to the TAMD and d-AFED schemes.

When $T_s = T$, the UFED scheme reduces to metadynamics[13] in its extended Lagrangian formulation, which includes extended variables coupled to the physical system[14,32] according to eq 7 and an adaptive bias potential similar to eq 5. Note that, in practice, we retain the coupling of the system to a heat bath in eq 7 in the limit of extended-Lagrangian metadynamics in order to prevent heating of the extended variables. This formulation of metadynamics differs from the (currently) most widely implemented formulation in which a bias potential similar to eq 5 acts directly on the CVs, $\mathbf{q}(\mathbf{r})$. The traditional proxy for metadynamics is the bias potential itself.[13] The PMF is estimated as $\phi_t^{\mathrm{hills}}(\mathbf{s}) = -u^{\mathrm{bias}}(\mathbf{s},t)$ after simulation time t. However, the precision of the PMF is limited by the hill size, with nondecreasing oscillations when large hills are added.[38] An improved hills-based PMF estimator[14,39] addresses this problem by averaging metadynamics results over time, starting from an initial filling time t_F

$$\phi_t^{\mathrm{hills,avg}}(\mathbf{s}) = -\frac{1}{t - t_F}\int_{t_F}^{t} \mathrm{d}t' u^{\mathrm{bias}}(\mathbf{s}, t') \tag{8}$$

An important alternative approach to improve the convergence of metadynamics, called well-tempered metadynamics,[24] relies on a modified adaptive bias potential

$$u^{\mathrm{bias,wt}}(\mathbf{s}, t) = \sum_{t_i<t} h\, \mathrm{e}^{-u^{\mathbf{bias,wt}}(\mathbf{s},t_i)/\Delta T}\, \mathrm{e}^{-(\mathbf{s}-\mathbf{s}(t_i))^2/2\sigma^2} \tag{9}$$

The key point of the method is that the rate at which the bias potential is added is decreased during the simulation proportional to $\exp(-u^{\mathrm{bias,wt}}(\mathbf{s},t)/\Delta T)$, where $T + \Delta T$ is called the pseudotemperature. In well-tempered medadynamics, the hills-based FES estimator takes the form

$$\phi_t^{\mathrm{hills,wt}}(\mathbf{s}) = -\frac{T + \Delta T}{\Delta T} u^{\mathrm{bias,wt}}(\mathbf{s}, t) \tag{10}$$

which derives from a formula introduced in refs 27 and 28 for recovering the free energy when the CVs are maintained at a temperature higher than the physical temperature.

In this study, we introduce a version of well-tempered metadynamics based on the extended Lagrangian formalism, which we believe has not been reported before. The equations of motion for this new formulation of well-tempered metadynamics are identical to eq 7 (including the coupling to a heat bath), except that the adaptive bias potential defined in eq 9 is used instead of eq 5. Note that the presence of the extended variables does not affect the validity of the FES estimator eq 10. Note also that the particular form of the bias potential has no impact on the general properties[31] of the UFED dynamics defined by eq 7.

At this point, we make an important observation about metadynamics and well-tempered metadynamics (in their Lagrangian form), as well as TAMD/d-AFED. Because these sampling methods are special cases of UFED, the force-based free energy estimator can trivially also be applied to them. A force-based estimator has, to our knowledge, never been used with these three methods and could present advantages in terms of convergence efficiency, which we propose to investigate.

Reweighted Ensembles from Dynamics with Adaptive Bias. The known above-mentioned shortcomings of the hill-based free energy estimator in metadynamics has prompted several authors to develop unbiasing schemes for histogram-based FES estimation and ensemble averages of arbitrary observables. The difficulty of the unbiasing scheme is to estimate the biased partition function in the interval between two hill deposition steps. Tiana[21] proposed a method using the

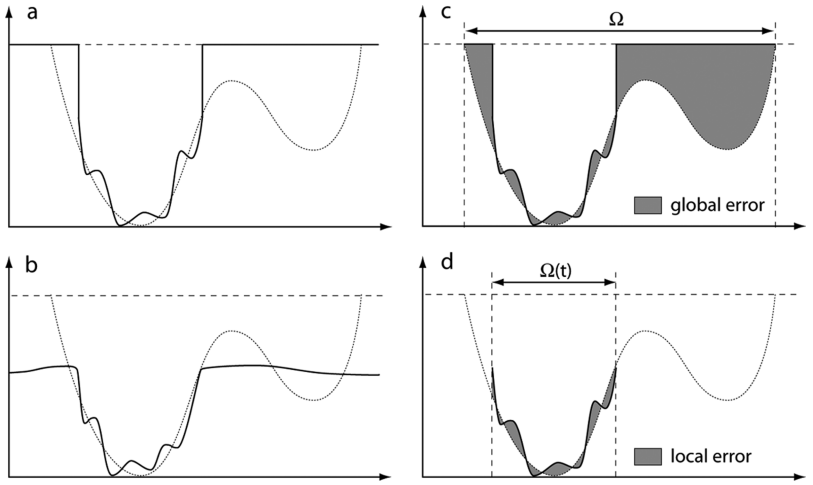

Figure 1. Schematic view of a partially sampled FES. (a) The histogram FES is truncated at a cutoff value (dashed line) in unsampled regions of the CV space (horizontal axis). (b) The force in unsampled regions is set to zero, which leads to an approximate plateau in the FES, much below the cutoff value. (c) The FES is set to the cutoff value in all unsampled regions. The *global error* (gray area) is calculated over the entire domain where the reference FES (dotted line) is below the cutoff. (d) The *local error* is calculated only on regions sampled so far in the simulation.

histogram in the locally sampled region and tested this proposal by calculating averages of one of the dihedral angles in the alanine dipeptide from a metadynamics simulation while using the other dihedral angle as a CV. Marinelli et al.[22] adapted the WHAM[4,5] method to unbias data from bias-exchange metadynamics and calculated NMR properties of the Trp-Cage peptide. Independently, Bonomi et al.[23] devised a similar method for well-tempered metadynamics[24] based on a differential equation representation of the histogram update, which circumvents the problem of calculating the biased partition function at each hill deposition step. The same authors[40] applied the method to compare calculated NMR scalar couplings of a 13-residue helix-forming peptide to experimental values.[40] We finally mention a general method by Athènes et al.[20] for unbiasing steered MD simulations, in which the steering can be performed by autonomous evolution of an extended degree of freedom.

Here, we build on the approach of Bonomi et al.[23] and extend it to the case of UFED with $T_s > T$. In this case, we restrict ourselves to the case of constant hill size, corresponding to standard (not well-tempered) metadynamics.[13,14] One notable difference with ref 23. is that we consider the adaptive bias potential to act on the meta-variable $\mathbf{s}$, not directly on the physical system. In the context of adiabatic dynamics, this is a significant difference, as the extended degrees of freedom evolve at high temperature.

The detailed derivation is given in Appendix A. Briefly, however, the biased, high-temperature state density $\rho_{\mathrm{adb}}^{\mathrm{bias}}(\mathbf{s},t)$ is accumulated during the simulation. At each hill deposition step, this density is updated as

$$\rho_{\mathrm{adb}}^{\mathrm{bias}}(\mathbf{s},\, t+\Delta t) = C(\mathbf{s},\, t,\, \Delta t)\rho_{\mathrm{adb}}^{\mathrm{bias}}(\mathbf{s},\, t)$$

The factor $C(\mathbf{s},t,\Delta t)$ is evaluated using the bias potential and the current estimate of the density. At final time τ, the FES can be obtained with the reweighed histogram estimator

$$\phi_{\tau}^{\mathrm{adb,bias}}(\mathbf{s}) = -k_{\mathrm{B}}T_s \ln[\rho_{\mathrm{adb}}^{\mathrm{bias}}(\mathbf{s},\, \tau)] - u^{\mathrm{bias}}(\mathbf{s},\, \tau) \qquad (11)$$

We note that for $u^{\mathrm{bias}} \equiv 0$ we recover eq 2, and for a uniform final density, $\rho_{\mathrm{adb}}^{\mathrm{bias}}(\mathbf{s},\tau) \equiv$ const, we recover the standard bias potential FES estimator of metadynamics. This provides a consistent set of histogram-based FES estimators for each of the sampling methods studied here, metadynamics, TAMD/d-AFED, and UFED.

Combining Information from the Histogram and the Force Using Kriging. For each sampling method, we now have both the histogram and the force as proxies for the estimation of the free energy. We will compare their efficiency below, but we can go one step further and ask whether combining information from both sources would yield faster convergence. For this, we need an estimator that combines observations of the values of a function (here the free energy, $\phi(\mathbf{s})$) and its derivatives (the mean force, $-\nabla\phi(\mathbf{s})$). The general idea is to use a differentiable basis set and fit both basis functions and their analytical derivatives at the same time. In many approaches, however, a parameter needs to be introduced to determine the relative importance lent to the derivative information.

An efficient and general regression method that solves this problem is kriging.[33,34] The philosophy behind the kriging method is to view the observations as realizations of a simple stochastic process of mean μ and variance σ. However, the observations are not independent, and the features of the target function are encoded in the correlations. These are expressed by the basis functions, usually multivariate Gaussians. The gradient-enhanced kriging (GEK) method[34,35] considers, in addition, the correlations between the data and the derivatives and between the derivatives and themselves. In Appendix B, we outline the principle of the method and present an adaptation to obtain a regularized version of GEK.

In practice, histogram and force data are accumulated on a grid in CV space before being fed to the regularized GEK algorithm. Special care must be taken for the data and derivatives to be consistent in and near unsampled regions. Typically, the mean force is set to zero, which creates large plateau regions, whereas the histogram tends to infinity in these regions (see next section). For this reason, we introduce an artificial cap to the histogram data, such that it is consistent with the plateau of the force-based FES. Note that the GEK method requires a numerical optimization in order to find the optimal Gaussian widths and regression parameter, a step that renders the computation of convergence curves computer

intensive when the number P of grid points is large because the dimension of the generalized correlation matrix is $[(n+1)P]^2$.

Measuring FES Convergence. A measure of the error with respect to a reference FES along the course of a simulation can serve different purposes. First, it can be used to compare the efficiency of various simulation algorithms to sample the entire CV space. Second, it can be used to assess the quality of various FES estimators given the sample obtained from a given simulation. For these two purposes, different kinds of error measures are required.

Particular attention must be given to regions of the CV space that belong to the domain of interest but have not been sampled by a simulation after a given time. Different FES reconstruction methods will behave very differently in these regions. The histogram FES goes to infinity in unsampled regions where the histogram is zero (see Figure 1a). In contrast, the mean force takes a default value of zero in the unsampled regions and integration leads to an approximately flat FES (see Figure 1b and the example FESs in Supporting Information Figures S1−S3). The FES reconstructed form the metadynamics hills behaves in a manner similar to the force FES. Regions where no hills have been deposited translate to a plateau that also increases with simulation time.

After a given simulation time t, let us define the sampled region $\Omega(t) = \{i \,|N_i(t) \geq N_{\min}\}$ as the set of bins i in the CV space that have been visited at least $N_{\min}$ times. The height of the aforementioned plateau outside of $\Omega(t)$ is arbitrary and is not relevant to the accuracy of the final FES. Therefore, for all FES estimators ϕ, we impose a cutoff value c outside of $\Omega(t)$

$$\bar{\phi}(i) = \begin{cases} \phi(i), & i \in \Omega(t) \\ c, & i \notin \Omega(t) \end{cases}$$

To assess the overall sampling efficiency of a simulation method, we define the *global error* with respect to a reference FES ϕ^{ref} over the entire domain of interest Ω, that is, the N_Ω bins where $\phi^{\text{ref}} < c$, as the L^1 norm

$$\varepsilon_{\text{global}} = \frac{1}{N_\Omega} \sum_{i \in \Omega} |\bar{\phi}(i) - \phi^{\text{ref}}(i)| \tag{12}$$

If c is high compared to the FES features, any unsampled bin will have a large contribution to $\varepsilon_{\text{global}}$, as shown on Figure 1c. In contrast, the *local error* pertains only to the region $\Omega(t)$ already sampled at time t (see Figure 1d), and is given by the L^1 norm

$$\varepsilon_{\text{local}} = \frac{1}{N_{\Omega(t)}} \sum_{i \in \Omega(t)} |\bar{\phi}(i) - \phi^{\text{ref}}(i)| \tag{13}$$

The local error is appropriate to compare different FES estimators independent of the sampling efficiency.

Computational Details. All simulations were performed with the Gromacs 4.5.5[41] software package. The alanine dipeptide in vacuo was modeled with the CHARMM22 force field[42] port to Gromacs.[43] All bonds were constrained, and the global translational and rotational displacements were set to zero at each step. All nonbonded interactions were computed without a cutoff. The molecule was coupled to a Nosé−Hoover chain thermostat[36] and equilibrated for 1 ns.

The Na^+ ion in water was modeled using the Gromos 43a5 force field[44] together with the SPC water model.[45] One ion was placed in a cubic periodic box with 759 water molecules. For extensive thermostatting, water molecules were divided into 256 groups, each of which was coupled to a Nosé−Hoover chain thermostat. The system was equilibrated for 1 ns at constant pressure using the Martyna−Tobias−Klein scheme[46] and further equilibrated for 1 ns at constant volume. During the constant volume calculation, the radial distribution function $\rho(\xi)$ of the centers of mass of the water molecules as a function of the distance ξ to the ion was calculated using the g_rdf program of the Gromacs suite.[41] The reference FES (excluding the Jacobian term) was then obtained as $\phi^{\text{ref}}(\xi) = -k_B T \log \rho(\xi)$. We note in passing that this system has been studied with steered MD in ref 47., however the authors did not consider calculating a reference FES from the radial distribution function, and the FES they reported for Na^+ is inaccurate.

All metadynamics, TAMD/d-AFED, and UFED calculations were performed with a modified version of the PLUMED 1.3 plugin.[48] In the metadynamics and TAMD/d-AFED simulations, the extended variables were coupled to a GGMT[37] thermostat with time constant 0.2 ps. In the UFED simulations, however, a Langevin thermostat was preferred. Indeed, the GGMT only scales the magnitude of a particle's velocity and does not enforce changes of sign, which can create artifacts for a single degree of freedom evolving at high temperature on a flat and periodic FES.

Hill summation and histogram reweighting use modified versions of the PLUMED auxiliary programs *sum_hills* and *reweight*,[48] respectively. The remaining postprocessing was done in MATLAB (MATLAB and Optimization Toolbox Release 2009b, MathWorks, Inc., Natick, Massachusetts, United States) using a suite of in-house scripts that is available for download on the author's web page (http://lausanne.isb-sib.ch/~mcuendet/software.html). The scripts are quite general and can be used to calculate FESs and convergence curves of dimension between one and four for any system using the histogram, the force, the hills, or kriging estimators. Third party routines are used for robust smoothing,[49] multidimensional force integration, and kriging.[34] Unless otherwise indicated, a uniform grid of 50 × 50 bins was used for the alanine dipeptide (see Figure 2) and 200 bins for the ion in water (see Figure 4).

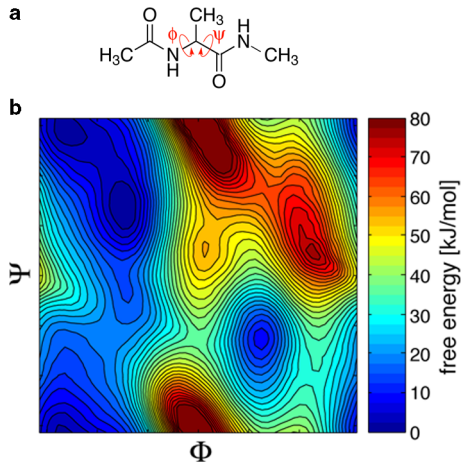

Figure 2. (a) Alanine dipeptide molecule with the usual Ramachandran dihedral angles Φ and Ψ. (b) FES in the (Φ,Ψ) plane form the UFED simulation (see text for details), reconstructed using eq 11 and the histogram reweighting technique described in Appendix A.

dx.doi.org/10.1021/ct500012b | J. Chem. Theory Comput. 2014, 10, 2975−2986

2. ALANINE DIPEPTIDE

We first look at the case of the alanine dipeptide in vacuo, the most widespread benchmark system for free energy methods. A summary of all simulations reported for this system is shown in Table 1 with relevant parameters. Unless otherwise indicated, simulations consist of five independent trajectories of 200 ns each. We present six main simulations: two metadynamics simulations, one with small hills (Meta1), one with large hills (Meta2), a well-tempered metadynamics simulation (Well1) with same initial hill size as Meta2, a TAMD/d-AFED simulation with T_s = 600 K (d-AFED1), a UFED simulation (UFED1) that combines the same small hills as Meta1 and same T_s as d-AFED1, and finally, a UFED simulation (UFED2) that uses the same large hills as Meta2 and T_s = 600 K. Note that the large hill heights of 2.0 kJ/mol are a factor of roughly four smaller than those used in ref 31, and despite a larger width, the hill volume is roughly 40% smaller. In addition, the hills are deposited every 10 ps here vs every 0.1 ps in ref 31. Thus, while we expect slower overall convergence, the main point here is to assess the *relative* performance of the FES estimators rather than to investigate the ability of the methods to achieve aggressive sampling, as was done in ref 31.

Table 1. Parameters for the Alanine Dipeptide Simulations[a]

	T_s [K]	m_s [amu·nnm^2/rad^2]	h [kJ/mol]	σ_h [rad]
Meta1	300	50	0.5	0.2
Meta2	300	50	2.0	0.314
Well1[b]	300	50	2.0	0.314
d-AFED1	600	50		
d-AFED2[c]	800	0.03−1000		
UFED1	600	500	0.5	0.2
UFED2	600	500	2.0	0.314
UFED3[d]	600	500	0.1	0.02

[a]Unless otherwise indicated, all simulations consist of 5 independent trajectories of 200 ns each with Δt = 2 fs and $\kappa_s = 10^3$ kJ·mol^{-1}·rad^{-2}. Hills are deposited every 10 ps. [b]This is a Lagrangian form of well-tempered metadynamics. The hill-scaling bias factor is 10, which corresponds to a pseudotemperature of 3000 K, see ref 24, but the extended variable was kept at 300 K. [c]10 simulations with increasing values of m_s. [d]Stiff coupling $\kappa_s = 2 \times 10^4$ kJ·mol^{-1}·rad^{-2} and reduced time step Δt = 0.2 fs.

To assess the effect of m_s on convergence speed and final accuracy, we performed an additional set of 10 trajectories (d-AFED2) with a range of m_s spanning 7 orders of magnitude. Finally a UFED simulation (UFED3) with a tighter coupling constant κ_s and a smaller time step provides insights on the effect of sampling rate and bin size on the accuracy of the force estimator.

The reference for the convergence plots is the FES obtained from the combined hills of the five Meta1 trajectories. The bias potential was divided by five, which results in very small hills (0.1 kJ/mol) yielding a high accuracy FES. The convergence curves shown in Figure 3 are averages over the convergence curves from the five independent trajectories of each simulation. The upper panels show the evolution of the global error, eq 12, and the lower panels show the local error, eq 13, for the same simulations.

The first general observation is that for a given simulation, the global error has a very uniform behavior across all estimators, except that the histogram method, which is slightly less efficient in the adiabatic simulations (d-AFED1, UFED1, and UFED2). Overall, sampling methods behave as expected, with Meta2 and UFED2 converging almost ten times faster than Meta1 and UFED1, respectively, which corresponds to the volume ratio between large and small hills. Accordingly, Well1 presents an intermediate global convergence speed.

In simulations with large hills (Meta2 and UFED2), the accuracy of the hills estimator is limited by the hill size, which is a well-known limitation of standard metaynamics.[38] In these simulations, the hill averaging estimator, eq 8 with a filling time t_F = 8 ns, resolves this issue, which is completely absent in the Well1 simulation, as expected. We note that the temperature increase makes the UFED simulations slightly more efficient for the chosen hill sizes than the metadynamics simulations with the same parameters if the force estimator is used. In ref 31, it was shown that larger hills and a higher hill deposition rate leads to a more significant improvement of UFED over standard metadynamics when the force estimator is used.

The local error shows differences among estimators in the regions already visited by the sampling algorithm. In all biased simulations, both the force and the reweighted histogram estimators outperform the hills estimator, as expected. The hill-averaging estimator is able to correct this trend toward the end of the simulation. While in all Meta1, Meta2, and Well1, the force and reweighed histogram estimators show comparable performance, the force estimator is significantly better in adiabatic simulations. Combining information from the force and the histogram using the kriging estimator seems to bring marginal improvements over the best single estimator, except in the case of TAMD/d-AFED, where the gain in accuracy is significant. In the case of UFED2, the modest accuracy of the reweighted histogram prevents the kriging estimator to reach the performance of the force estimator.

In adiabatic free energy methods, the most critical parameter is the extended variable mass. It should be chosen high enough for effective adiabatic decoupling between the physical and extended systems and low enough to allow sufficient sampling in the planned simulation time. The physical mass to which m_s should be compared is m_{eff} as estimated from eq 4. For the alanine dipeptide, $m_{\text{eff}} \approx 0.03$ amu·nm^2/rad^2. To quantify adiabaticity, we recorded the heat transfer rate from the extended system to the physical system, calculated from the work of the coupling force

$$W_s(\tau) = \int_0^\tau \mathrm{d}t\ \kappa_s(\mathbf{q}(\mathbf{r}) - \mathbf{s})\frac{p_s}{m_s} \tag{14}$$

A natural question to ask concerns the impact of m_s on the convergence properties. The d-AFED2 simulation consists of 10 trajectories with m_s ranging from 0.03 to 1000 amu·nm^2/rad^2. Figure 4a shows a linear relation between the log δW_s and log m_s. Figure 4b shows the convergence curves obtained in the d-AFED2 set of trajectories with the force estimator. For masses below 100 m_{eff}, the FES does not converge to ϕ^{ref} because the adiabatic separation is not effective. As the mass is increased further (for δW_s lower than a few kJ/mol/ps), the final FES is correct, but the convergence speed decreases. This trade-off is illustrated in Figure 4c, which overlays curves of the final FES error and the simulation time necessary for the global error to drop below 10 kJ/mol. We see that m_s values between 100 and 1000 m_{eff} offer a good compromise.

The force and the histogram data are very different in terms of the time scale of the autocorrelation function. The decorrelation time of the collective variable used in the

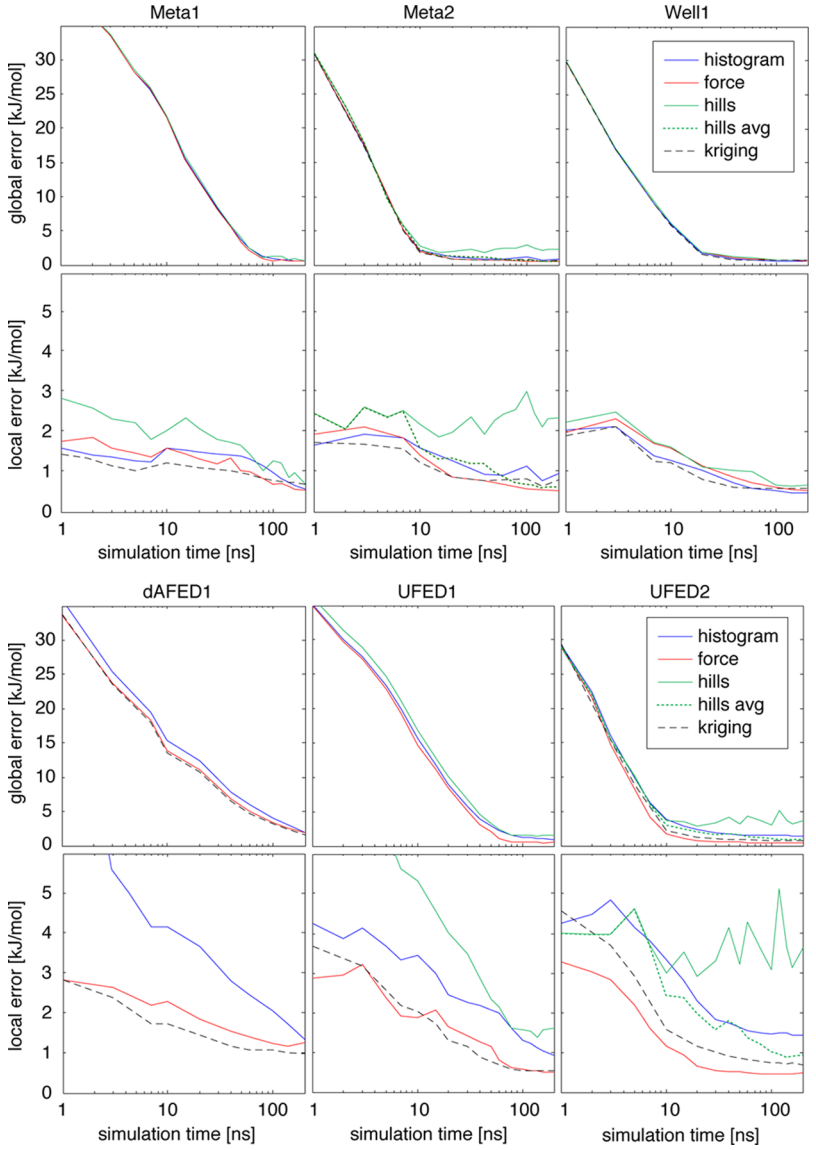

Figure 3. Convergence of the FES for the alanine dipeptide using various free energy estimators and sampling methods as described in 1. For d-AFED, the error is computed where $\Delta G^{ref} < 40$ kJ/mol and for all other methods where $\Delta G^{ref} < 60$ kJ/mol.

histogram is long due to the large m_s. On the other hand, the force oscillates fast due to the tight coupling constant κ_s. A way to improve the force estimator convergence could be to choose a high value of κ_s and increase the sampling rate to take advantage of very short decorrelation times. This might require the use of a multiple time step type of integrator with a small time step for this stiff harmonic coupling.[26,50] This can be achieved without significantly affecting the efficiency of the calculation. The gain in sampling is, however, balanced by the increased noise due to the amplitude of the force oscillations. The estimator behavior will also depend on the bin size, larger bins allowing for more noise cancellation.

In order to gain insights on the trade-off between sampling rate and bin size, we performed the UFED3 simulation with a value of κ_s 20 time higher than for other simulations in this study. We decreased the time step to 0.2 fs and collected 10 times more samples (every 10 fs). We applied the histogram and force estimators with increasing sample stride, defined as the number of data points left out between samples used. Figure 5 shows that, as expected, the histogram estimator is not very much affected. On the other hand, the error of the force estimator strongly increases past a certain threshold of sample stride. With 50 bins and stride 10, the local error turns out to be the same as the final error of the UFED1 simulation shown in Figure 3, which shows that no improvement would have been obtained by increasing κ_s and sampling rate in the UFED1 simulation.

3. ION IN WATER

As a second benchmark, we consider the free energy profile of a water molecule as a function of its distance to a sodium ion (see Figure 6a). The natural one-dimensional CV is the distance between the ion and the center of mass of one water molecule. This example can be seen as a basic prototype for binding reactions in explicit solvent. It is a more difficult exercise than the alanine dipeptde for several reasons. First, there are many slow-relaxing degrees of freedom orthogonal to the CV. Second, features on the FES are only a few kJ/mol in height (see Figure 6b), so that a higher precision is required with respect to k_BT. Third, the CV domain of interest extends over

dx.doi.org/10.1021/ct500012b | J. Chem. Theory Comput. 2014, 10, 2975−2986

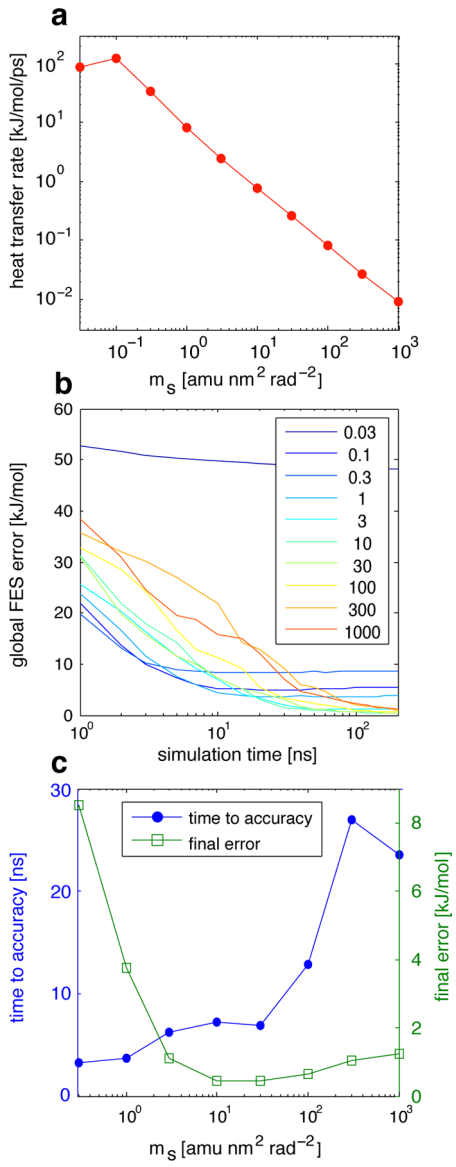

Figure 4. (a) Heat transfer rate between the extended system and the physical system as a function of m_s, estimated using eq 14 in the d-AFED2 simulation with m_s ranging from 0.03 to 1000 amu·nm^2/rad^2. (b) Convergence of the global error with varying m_s (see legend for color code) using the force estimator. (c) Simulation time necessary to beat 10 kJ/mol global error (left axis) and final error after 200 ns (right axis), as functions of m_s.

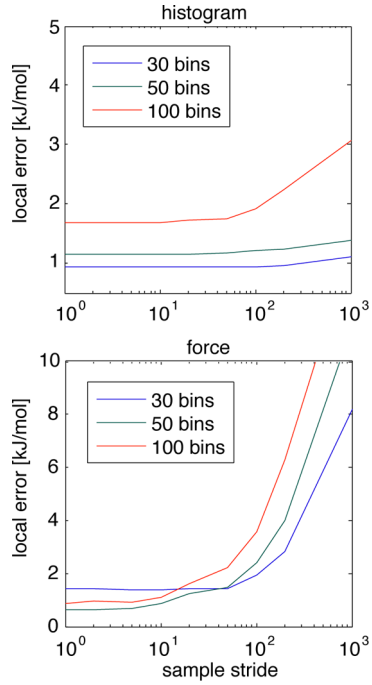

Figure 5. Evolution of the error as the stride between sample points is increased in the alanine dipeptide simulation UFED3, which has a high coupling constant and a time step 10 times smaller than other simulations.

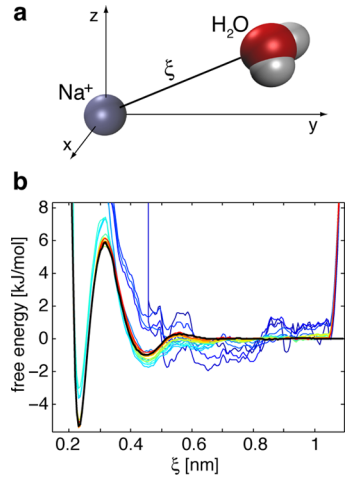

Figure 6. (a) Water molecule in the vicinity of a sodium ion. The system comprises 758 other water molecules (not shown) with periodic boundary conditions. (b) Convergence of the free energy profile from the UFED1 simulation with the force FES estimator. The simulation time increases from blue curves to red curves, up to the total simulation time of 50 ps. The thick black line represents the reference FES obtained from the radial distribution function.

approximately 0.9 nm, but the main feature (the global minimum) is extremely narrow (about 0.02 nm) and strong gradients are present.

For the ion in water system, we performed one metadynamics, one well-tempered metadynamics, one TAMD/d-AFED, and one UFED simulation with parameters shown in Table 2. In order to capture accurately the sharp FES features, a tight coupling constant, $\kappa_s = 5 \times 10^5$ kJ·mol^{-1}·nm^{-2}, was required. Equation 4 gives an effective mass of 10.10 amu for the CV, which translates into a typical period of $2\pi(m_{\text{eff}}/\kappa_s)^{1/2} \approx 0.028$ ps for the extended variable coupling. This is too short for accurate integration with the standard MD time step of 2 fs. Therefore, a dual time-step algorithm similar to the RESPA[50] scheme was used with a time step of 0.2 fs for the extended variable coupling term and 2 fs for the physical system. Again, each simulation consists of five independent trajectories.

The convergence curves for the ion in water simulations are shown in Figure 7. The reference FES, represented by a black line in Figure 6b is calculated from the radial distribution function of all water molecules. For this system we show only the global error, eq 12, because the local error is almost identical after 1 ns of simulation time. This is due to the fact that the system is mostly diffusive in nature with relatively low free energy barriers. In such a system with a single one-

dx.doi.org/10.1021/ct500012b | J. Chem. Theory Comput. 2014, 10, 2975−2986

Table 2. Parameters for the Ion in Water Simulations[a]

	T_s [K]	m_s amu	h [kJ/mol]	σ_h nm
Meta	300	10^4	0.2	0.02
Well[b]	300	10^4	0.2	0.02
d-AFED	800	10^5		
UFED	600	10^4	0.1	0.02

[a]All simulations consist of five independent trajectories of 50 ns each. Here, $\kappa_s = 5 \times 10^5$ kJ·mol^{-1}·nm^{-2}, which required a time step of Δt = 0.2 fs for the extended variable coupling, while physical interactions were integrated with the usual 2 fs time step. Hills were deposited every 2 ps. [b]This is a Lagrangian form of well-tempered metadynamics. The hill-scaling bias factor is 5, which corresponds to a pseudotemperature of 1500 K (see ref 24), but the extended variable was kept at 300 K.

dimensional CV, all relevant regions of the CV space are discovered early in the simulation. The difficulty then is to sample all relevant conformations of the orthogonal degrees of freedom for the FES to converge.

In both the metadynamics and the UFED simulations, we observe, once more, that the hills estimator does not converge to the reference FES, whereas the hills-averaging estimator, eq 8 does. We also note that the final accuracy of the histogram estimator is slightly worse in the TAMD/d-AFED case, which may be due to the fact that the unbiasing, eq 2, is sensitive to the effective temperature of the CV, in particular when a temperature-dependent Jacobian correction is applied.

In terms of convergence speed, we see that the force estimator is substantially superior to others in all four types of simulations. With this estimator, under similar conditions, UFED is the most performant method, reaching the 1 kJ/mol mark after 8 ns, followed by dAFED and well-tempered metadynamics, after 15 ns. It turns out that for this system, the idea of combining the force and histogram estimators does not pay off. If large discrepancies occur between the derivative and the data information, the kriging algorithm tends to fold back to the histogram estimator. In this case, a simple or Bayesian average of the force and histogram FES performs better than kriging (data not shown). It should be noted, however, that in the absence of a reference calculation, it might not be obvious which estimator has the best performance, and a simple average or kriging combination of the force and the histogram estimators will generally yield a result better than the worse of the two.

4. CONCLUSION

In this work, we started from the realization that for a given sampling method, either metadynamics, well-tempered metadynamics, TAMD/d-AFED, or UFED, a variety of different estimators can be used to construct the FES. These estimators are based on different proxies, namely the histogram, the mean force, the biasing potential (if applicable), or a combination of force and histogram. For the first time to our knowledge, we combined a mean force FES estimator with metadynamics and well-tempered metadynamics. In addition, we showed that a histogram-based estimator can be used together with the general UFED sampling scheme, via a proper reweighting scheme. In addition, we have introduced an extended-Lagrangian version of well-tempered metadynamics, which has not been reported previously. For both the alanine dipeptide in solution and the sodium ion in water, we systematically examined the convergence properties of each FES estimator in association with each sampling method.

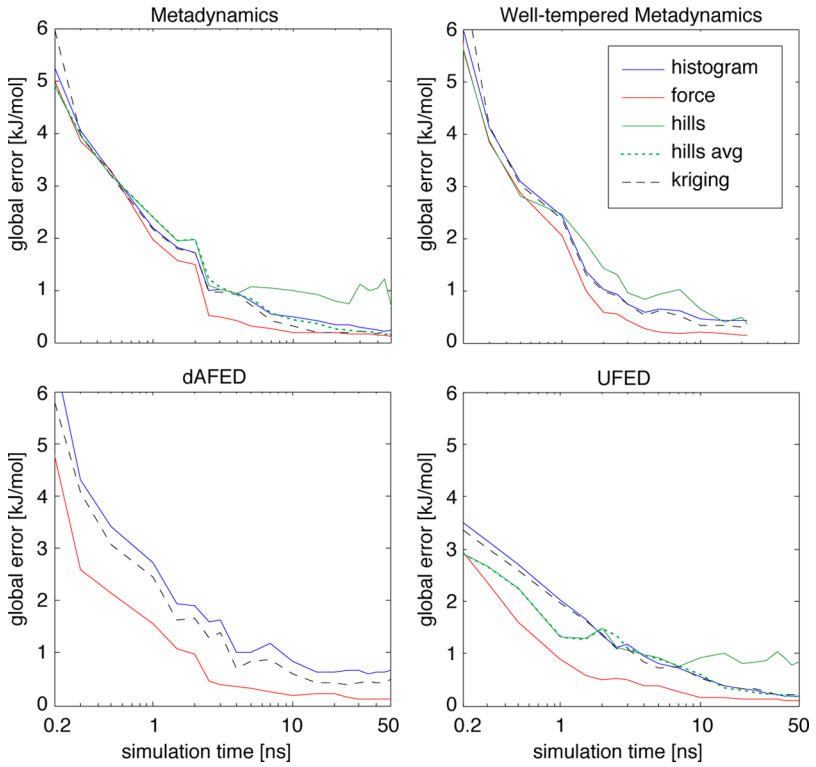

Figure 7. Convergence of the FES as a function of distance between a water molecule and a Na^+ ion. Convergence curves are averaged over five independent trajectories of length ranging from 0.2 to 50 ns.

dx.doi.org/10.1021/ct500012b | J. Chem. Theory Comput. 2014, 10, 2975−2986

A central result of this paper is that the force estimator is superior to others in all simulations that we reported. This finding is particularly interesting in the case of metadynamics and TAMD/d-AFED, in which the force estimator is not commonly used. In metadynamics and well-tempered metadynamics, this advantage warrants the implementation of the slightly more complicated extended Lagrangian formulation that involves integrating the equation of motion of an extended variable. As a result, the mean force is a direct output of the simulation. In the postprocessing stage, direct numerical integration of the mean force works well for low-dimensional CVs. In higher dimensions, more advanced integration techniques are required, such as the sparse binning scheme introduced with the UFED method.[31]

We observed that the idea of combining information from the force and the histogram can lead to a moderately improved FES estimator only when the force and histogram samples are of comparable quality. In case of a discrepancy, the kriging algorithm tends to trust the histogram more, which is not the best estimator in the cases reported here. The fact that the improvement is moderate could be attributed to the fact that the kriging approach or its implementation are not optimal. For example, one could imagine a combined estimator that directly exploits individual sample points instead of data accumulated on a grid. However, our findings are similar to those obtained in a study that came out at the time of submission of this paper, which uses Bayesian Gaussian process regression approach to combine force and histogram information.[51]

Finally, one striking feature is the overall similarity of the global error decay of the different FES estimators for a given set of trajectories, as well as the generally low values of the local error. This suggests that the simple fact that the system visits a given region of space is more important than the nature of the particular estimator used to calculate the FES. This might also have deeper implications about the amount of independent information contained in the various estimators. The fact that the gain from combining force and histogram information is moderate can be taken as an indicator that the two proxies are closely dependent from each other. While we do expect the force and histogram to be globally consistent, it is not obvious that they should be so on short time scales along a single trajectory. It should be noted that the trends observed in this study might be highly system dependent. In future work, similar FES estimator assessments will be performed on larger and more complex systems with much richer structure and time scales in the space orthogonal to the CVs.

APPENDIX A: REWEIGHTING THE UFED ENSEMBLE

The derivation follows that of ref 23 but diverges from it because the bias acts on the extended variables instead of the physical degrees of freedom. In this case, the influence of the physical system on the dynamics of $\mathbf{s}$ is still represented by the unmodified PMF $\phi(\mathbf{s})$. However, the distribution of $\mathbf{s}$ will be biased by $u^{\text{bias}}(\mathbf{s},t)$.

In the context of adiabatic dynamics, the extended variable evolves at temperature $T_s > T$, with $\beta_s = 1/k_B T_s$. Choosing a large mass m_s for $\mathbf{s}$ ensures that there is a sufficient time scale difference to have effective adiabatic separation between physical and extended systems. If, in addition, we assume that the system is at equilibrium at time t between two hill depositions, we can write the biased adiabatic density for $\mathbf{s}$,

$$\rho_{\text{adb}}^{\text{bias}}(\mathbf{s},\, t) = \frac{\mathrm{e}^{-\beta_s[\phi(\mathbf{s})+u^{\text{bias}}(\mathbf{s},t)]}}{\int d\mathbf{s}\, \mathrm{e}^{-\beta_s[\phi(\mathbf{s})+u^{\text{bias}}(\mathbf{s},t)]}}$$

If we now multiply and divide by $\int d\mathbf{s}\, \mathrm{e}^{-\beta_s\phi(\mathbf{s})}$ and rearrange, we obtain

$$\rho_{\text{adb}}^{\text{bias}}(\mathbf{s},\, t) = \mathrm{e}^{-\beta_s u(\mathbf{s},t)} \frac{\int d\mathbf{s} \mathrm{e}^{-\beta_s\phi(\mathbf{s})}}{\int d\mathbf{s} \mathrm{e}^{-\beta_s[\phi(\mathbf{s})+u^{\text{bias}}(\mathbf{s},t)]}} \frac{\mathrm{e}^{-\beta_s\phi(\mathbf{s})}}{\int d\mathbf{s} \mathrm{e}^{-\beta_s\phi(\mathbf{s})}}$$

$$= \mathrm{e}^{-\beta_s u(\mathbf{s},t)} \langle \mathrm{e}^{-\beta_s u^{\text{bias}}(\mathbf{s},t)} \rangle_{\text{adb}}^{-1} \rho_{\text{adb}}(\mathbf{s})$$

Here, $\rho_{\text{adb}}(\mathbf{s})$ represents the adiabatic distribution at inverse temperature β_s as it appears in the TAMD/d-AFED method[26] and $\langle\cdot\rangle_{\text{adb}}$ is the corresponding ensemble average. This procedure is a simplified version of the standard umbrella sampling unbiasing[52] that is used when the bias potential acts directly on the physical variables as in ref 23. From the second term on the right-hand side, we define the auxiliary function

$$c(t) \doteq -\frac{1}{\beta_s} \ln \langle \mathrm{e}^{-\beta_s u^{\text{bias}}(\mathbf{s},t)} \rangle_{\text{adb}}^{-1}$$

This function is very similar to that defined in ref 23, except that it involves β_s instead of β. We now have

$$\rho_{\text{adb}}^{\text{bias}}(\mathbf{s},\, t) = \mathrm{e}^{-\beta_s[u(\mathbf{s},t)+c(t)]} \rho_{\text{adb}}(\mathbf{s}) \tag{15}$$

This relation expresses the biased adiabatic density at time t in terms of the constant, unbiased adiabatic density. From eq 15, we can determine an expression for the biased adiabatic distribution at time $t + \Delta t$ as a function of the distribution at time t,

$$\rho_{\text{adb}}^{\text{bias}}(\mathbf{s},\, t+\Delta t) = \mathrm{e}^{-\beta_s[\dot{c}(t)+\dot{u}^{\text{bias}}(\mathbf{s},t)]\Delta t} \rho_{\text{adb}}^{\text{bias}}(\mathbf{s},\, t) \tag{16}$$

It is straightforward to show that

$$\dot{c}(t) = -\int d\mathbf{s} \dot{u}^{\text{bias}}(\mathbf{s},\, t) \rho_{\text{adb}}^{\text{bias}}(\mathbf{s},\, t) = -\langle \dot{u}^{\text{bias}}(\mathbf{s},\, t) \rangle_{\text{adb}}^{\text{bias}} \tag{17}$$

This biased average in the adiabatic ensemble is available during the simulation. The time derivative of the bias potential is always zero, except at the time t_i when a new Gaussian is added. At this instant, we have

$$\dot{u}^{\text{bias}}(\mathbf{s},\, t_i) = \frac{h}{\Delta t} \mathrm{e}^{-(\mathbf{s}-\mathbf{s}(t_i))^2/2\sigma^2}$$

Because this function is local around the current position $\mathbf{s}(t_i)$, the evaluation of eq 17 is facilitated. Finally, the algorithm goes as follows:

Algorithm

1. At each step between Gaussian depositions, update the histogram $\rho_{\text{adb}}^{\text{bias}}(\mathbf{s},t)$.
2. At $t = t_i$, add a new Gaussian at $\mathbf{s}(t_i)$ and update $\rho_{\text{adb}}^{\text{bias}}(\mathbf{s},t)$ according to eq 16, using eq 17 to estimate $\dot{c}(t)$ using the current empirical density.
3. At final time τ, recover the unbiased, temperature-corrected density by inverting eq 15 and applying the usual TAMD/d-AFED distribution rescaling,

$$\rho(\mathbf{s}) \propto [\rho_{\text{adb}}^{\text{bias}}(\mathbf{s},\, \tau)]^{\beta/\beta_s} \mathrm{e}^{+\beta u^{\text{bias}}(\mathbf{s},\tau)}$$

APPENDIX B: REGULARIZED GRADIENT-ENHANCED KRIGING

Kriging is essentially a parameter-free method to build a surrogate for a function $f(\mathbf{x})$ of M-dimensional variables $\mathbf{x} = (x_1,...,x_M)$ based on n observations denoted $\mathbf{y} = (y(\mathbf{x}^1),...,y(\mathbf{x}^n))$. In the context of the rest of the present paper, f represents the free energy and $\mathbf{x}$ the position in CV space. The surrogate function will be constructed as a combination of basis functions of the form

$$\psi^i(\mathbf{x}) = \exp\left(-\sum_{k=1}^{M} \theta_k (x_k^i - x_k)^2\right) \tag{18}$$

Here, different components of $\boldsymbol{\theta} = (\theta_1,...,\theta_M)$ allow the width of the basis functions to be different for each variable. The underlying stochastic process is assumed to be Gaussian with mean μ and variance σ, $y \sim \mathcal{N}(\mu, \sigma)$. The random variables are correlated with each other according to the basis function expression, eq 18. From the observations, we can build the correlation matrix $\boldsymbol{\psi}$ with components

$$\boldsymbol{\psi}_{ij} = \mathrm{cor}[y(\mathbf{x}^i), y(\mathbf{x}^j)] = \exp(-\sum_{k=1}^{M} \theta_k |x_k^i - x_k^j|^2)$$

The value of $\boldsymbol{\theta}$ is optimized to maximize the likelihood of y within this model. A new prediction $\hat{y}$ at $\mathbf{x}$ is then chosen such that it maximizes the likelihood of both the sample data and the prediction itself. Define the vector $\boldsymbol{\psi}$ of correlations of the prediction with the observed data with components $\psi^i = \mathrm{cor}[y(\mathbf{x}^i),\hat{y}(\mathbf{x})]$. The maximum likelihood estimate for the prediction can then be expressed as

$$\hat{y} = \hat{\mu} + \boldsymbol{\psi}^T \boldsymbol{\psi}^{-1}(\mathbf{y} - \mathbf{1}\hat{\mu})$$

Note that in this simplest form, Kriging is merely an interpolation method (i.e., $\hat{y}(\mathbf{x}^i) = y(\mathbf{x}^i)$). However, the method can be easily regularized by adding a regression constant λ to the diagonal of the correlation matrix. We now have $\boldsymbol{\psi}+\lambda\mathbf{I}$, with $\mathbf{I}_n$ a $n \times n$ identity matrix, such that $\mathrm{cor}[y(\mathbf{x}^i),y(\mathbf{x})] = 1 + \lambda$ as $\mathbf{x} \to \mathbf{x}^i$. The regression parameter λ is estimated by maximum likelihood at the same time as $\boldsymbol{\theta}$.

Among all existing regression methods, Kriging has the advantage that it can be easily extended to include gradient information at each sample point.[34,35] In gradient-enhanced Kriging (GEK), observations take the form

$$\tilde{y}(\mathbf{x}^i) = \left(f(\mathbf{x}^i), \frac{\partial f}{\partial x_1}(\mathbf{x}^i), ..., \frac{\partial f}{\partial x_M}(\mathbf{x}^i)\right)$$

The $n \times M$ additional basis functions used to incorporate the gradient information are simply the derivatives $\partial\psi^j/\partial x_k^i$ of the n original Gaussian basis functions in eq 18. The extended correlation matrix $\tilde{\boldsymbol{\psi}}$ must include the correlations between the data, the data and the gradients, and the gradients and themselves. We constructed the correlation matrix as follows (shown for a one-dimensional problem in the interest of conciseness),

$$\tilde{\boldsymbol{\psi}} = \begin{pmatrix} \boldsymbol{\psi} + \lambda\mathbf{I}_n & \dfrac{\partial \boldsymbol{\psi}}{\partial x^i} \\ \dfrac{\partial \boldsymbol{\psi}}{\partial x^j}^T & \dfrac{\partial^2 \boldsymbol{\psi}}{\partial x^i \partial x^j} + 2\theta\lambda\mathbf{I}_n \end{pmatrix}$$

Note that the regression parameter for derivatives cannot have the same units as for the data itself. Given the fact that

$$\frac{\partial^2 \boldsymbol{\psi}^{ij}}{\partial x^i \partial x^j} = [2\theta + 4\theta^2(x^i - x^j)^2]\boldsymbol{\psi}^{ij}$$

we chose to define the regression parameter as $2\theta\lambda$ for derivatives, in order to keep a single parameter λ to optimize. Other choices are possible, including defining separate values $\lambda_1,...,\lambda_M$ for each of the derivatives, that need to be optimized in addition to λ. The latter solution was preferred for the ion in water system, in which the single λ optimization turned out to be unstable in some cases, leading to strong oscillations in the FES.

The construction of $\tilde{\boldsymbol{\psi}}$ generalizes seamlessly to higher dimensions and finally the regularized GEK prediction is obtained as

$$\hat{y} = \hat{\mu} + \tilde{\boldsymbol{\psi}}^T \tilde{\boldsymbol{\psi}}^{-1}(\mathbf{y} - \mathbf{1}\hat{\mu})$$

where $\tilde{\boldsymbol{\psi}} = (\boldsymbol{\psi}, \partial\boldsymbol{\psi}/\partial x_1,...,\partial\boldsymbol{\psi}/\partial x_M)$.

The method was implemented in MATLAB by modifying the Kriging package provided by Forrester et al.[34] The optimization of $\boldsymbol{\theta}$ and λ was performed using the active-set algorithm of the constrained nonlinear optimization function in MATLAB 2009.

ASSOCIATED CONTENT

Supporting Information

Three supplementary figures illustrating how the FES converges over the course of a UFED2 simulation (see Table 1) for the alanine dipeptide in vacuo with the CHARMM22 force field. Three different FES estimators used to construct the FES: in Figure S1 the reweighted histogram estimator, in Figure S2 the force, and in Figure S3 the metadynamics hills. This material is available free of charge via the Internet at http://pubs.acs.org

AUTHOR INFORMATION

Corresponding Author

*Email: mark.tuckerman@nyu.edu.

Notes

The authors declare no competing financial interest.

ACKNOWLEDGMENTS

This work has been partly funded by Fellowship PA00P2_129092 of the Swiss National Science Foundation for M.A.C and the U.S. National Science Foundation grant CHE-1301314 for M.E.T. We are grateful to M. Chen for insightful discussions. Computations were performed at the Vital-IT (http://www.vital-it.ch) Center for high-performance computing of the SIB Swiss Institute of Bioinformatics.

REFERENCES

(1) Christen, M.; van Gunsteren, W. F. *J. Comput. Chem.* **2007**, *29*, 157.

(2) Chipot, C., Pohorille, A., Eds. *Free Energy Calculations, Theory and Applications in Chemistry and Biology*; Springer Series in Chemical Physics; Springer Series in Chemical Physics; Springer: Berlin, 2007; Vol. *86*.

(3) Torrie, G. M.; Valleau, J. P. *J. Comput. Phys.* **1977**, *23*, 187−199.

(4) Kumar, S.; Bouzida, D.; Swendsen, R. H.; Kollman, P. A.; Rosenberg, J. M. *J. Comput. Chem.* **1992**, *13*, 1011−1021.

(5) Kumar, S.; Rosenberg, J.; Bouzida, D.; Swendsen, R.; Kollman, P. *J. Comput. Chem.* **1995**, *16*, 1339−1350.

(6) Carter, E. A.; Ciccotti, G.; Hynes, J. T.; Kapral, R. *Chem. Phys. Lett.* **1989**, *156*, 472−477.
(7) Sprik, M.; Ciccotti, G. *J. Chem. Phys.* **1998**, *109*, 7737−7744.
(8) Kirkwood, J. G. *J. Chem. Phys.* **1935**, *3*, 300−313.
(9) Darve, E.; Pohorille, A. *J. Chem. Phys.* **2001**, *115*, 9169−9183.
(10) Hénin, J.; Chipot, C. *J. Chem. Phys.* **2004**, *121*, 2904−2914.
(11) Minary, P.; Tuckerman, M. E.; Martyna, G. J. *SIAM J. Sci. Comput.* **2008**, *30*, 2055−2083.
(12) Zhu, Z.; Tuckerman, M. E. *Phys. Rev. Lett.* **2002**, *88*, 100201.
(13) Laio, A.; Parrinello, M. *Proc. Nat. Acad. Sci.* **2002**, *99*, 12562−12566.
(14) Laio, A.; Gervasio, F. L. *Rep. Prog. Phys.* **2008**, *71*, 126601.
(15) Jarzynski, C. *Phys. Rev. Lett.* **1997**, *78*, 2690−2693.
(16) Vanden-Eijnden, E.; Venturoli, M. *J. Chem. Phys.* **2009**, *130*, 194101−194101.
(17) Kästner, J.; Thiel, W. *J. Chem. Phys.* **2005**, *123*, 144104.
(18) Khavrutskii, I.; Dzubiella, J.; McCammon, J. *J. Chem. Phys.* **2008**, *128*, 044106.
(19) Maragliano, L.; Vanden-Eijnden, E. *J. Chem. Phys.* **2008**, *128*, 184110.
(20) Athènes, M.; Marinica, M. *J. Comput. Phys.* **2010**, *229*, 7129−7146.
(21) Tiana, G. *Eur. Phys. J. B* **2008**, *63*, 235−238.
(22) Marinelli, F.; Pietrucci, F.; Laio, A.; Piana, S. *PLoS Comput. Biol.* **2009**, *5*, e1000452.
(23) Bonomi, M.; Barducci, A.; Parrinello, M. *J. Comput. Chem.* **2009**, *30*, 1615−1621.
(24) Barducci, A.; Bussi, G.; Parrinello, M. *Phys. Rev. Lett.* **2008**, *100*, 020603 .
(25) Maragliano, L.; Vanden-Eijnden, E. *Chem. Phys. Lett.* **2006**, *426*, 168−175.
(26) Abrams, J. B.; Tuckerman, M. E. *J. Phys. Chem. B* **2008**, *112*, 15742−15757.
(27) Rosso, L.; Tuckerman, M. E. *Mol. Simul.* **2002**, *28*, 91−112.
(28) Rosso, L.; Minary, P.; Zhu, Z. W.; Tuckerman, M. E. *J. Chem. Phys.* **2002**, *116*, 4389−4402.
(29) VandeVondele, J.; Roethlisberger, U. *J. Phys. Chem. B* **2002**, *106*, 203−208.
(30) Cuendet, M. A.; Tuckerman, M. E. *J. Chem. Theory Comput.* **2012**, *8*, 3504−3512.
(31) Chen, M.; Cuendet, M. A.; Tuckerman, M. E. *J. Chem. Phys.* **2012**, *137*, 024102.
(32) Iannuzzi, M.; Laio, A.; Parrinello, M. *Phys. Rev. Lett.* **2003**, *90*, 238302.
(33) Krige, D. G. *J. Chem., Metall. Min. Eng. Soc. South Africa* **1951**, *52*, 119−139.
(34) Forrester, A. I. J.; Sóbester, A.; Keane, A. J. *Design via Surrogate Modelling: A Practical Guide*; John Wiley & Sons, Chichester, U.K., 2008.
(35) Mardia, K.; Kent, J.; Goodall, C.; Little, J. *Biometrika* **1996**, *83*, 207−221.
(36) Martyna, G. J.; Klein, M. L.; Tuckerman, M. *J. Chem. Phys.* **1992**, *97*, 2635−2643.
(37) Liu, Y.; Tuckerman, M. E. *J. Chem. Phys.* **2000**, *112*, 1685−1700.
(38) Laio, A.; Rodriguez-Fortea, A.; Gervasio, F.; Ceccarelli, M.; Parrinello, M. *J. Phys. Chem. B* **2005**, *109*, 6714−6721.
(39) Crespo, Y.; Marinelli, F.; Pietrucci, F.; Laio, A. *Phys. Rev. E* **2010**, *81*, 55701.
(40) Barducci, A.; Bonomi, M.; Parrinello, M. *Biophys. J.* **2010**, *98*, L44−L46.
(41) Pronk, S.; Páll, S.; Schulz, R.; Larsson, P.; Bjelkmar, P.; Apostolov, R.; Shirts, M. R.; Smith, J. C.; Kasson, P. M.; van der Spoel, D.; Hess, B.; Lindahl, E. *Bioinformatics* **2013**, *29*, 845−854.
(42) MacKerell Jr., A.; Brooks III, C.; Nilsson, L.; Roux, B.; Won, Y.; Karplus, M. In *CHARMM: The Energy Function and Its Parameterization with an Overview of the Program*; v. R. Schleyer, P. et al., Ed.; The Encyclopedia of Computational Chemistry; John Wiley & Sons: Chichester, 1998; Vol. *1*; pp 271−277.
(43) Bjelkmar, P.; Larsson, P.; Cuendet, M.; Hess, B.; Lindahl, E. *J. Chem. Theory Comput.* **2010**, *6*, 459−466.
(44) van Gunsteren, W. F.; Billeter, S. R.; Eising, A. A.; Hünenberger, P. H.; Krüger, P.; Mark, A. E.; Scott, W. R. P.; Tironi, I. G. *Biomolecular Simulation: The GROMOS96 Manual and User Guide*; Vdf Hochschulverlag AG an der ETH Zürich: Zürich, Switzerland, 1996.
(45) Smith, P. E.; van Gunsteren, W. F. *J. Chem. Phys.* **1994**, *100*, 3169.
(46) Martyna, G. J.; Tobias, D. J.; Klein, M. L. *J. Chem. Phys.* **1994**, *101*, 4177.
(47) Cascella, M.; Guidoni, L.; Maritan, A.; Rothlisberger, U.; Carloni, P. *J. Phys. Chem. B* **2002**, *106*, 13027.
(48) Bonomi, M.; Branduardi, D.; Bussi, G.; Camilloni, C.; Provasi, D.; Raiteri, P.; Donadio, D.; Marinelli, F.; Pietrucci, F.; Broglia, R.; Parrinello, M. *Comput. Phys. Commun.* **2009**, *180*, 1961−1972.
(49) Garcia, D. *Comput. Stat. Data Anal.* **2010**, *54*, 1167−1178.
(50) Tuckerman, M.; Berne, B. J.; Martyna, G. J. *J. Chem. Phys.* **1992**, *97*, 1990.
(51) Stecher, T.; Bernstein, N.; Csányi, G. *arXiv:1312.4419 [cond-mat.stat-mech]* **2013**.
(52) van Gunsteren, W. F.; Beutler, T. C.; Fraternali, F.; King, P. M.; Mark, A. E.; Smith, P. E. In *Computer Simulation of Biomolecular Systems, Theoretical and Experimental Applications*; van Gunsteren, W. F., Weiner, P. K., Wilkinson, A. J., Eds.; Escom Science Publishers: Leiden, The Netherlands, 1993; Vol. *2*; pp 315−348.